Available online at www.sciencedirect.com
SCIENCE DIRECT®
ELSEVIER
Nuclear Instruments and Methods in Physics Research A 553 (2005) 501–511
NUCLEAR INSTRUMENTS & METHODS IN PHYSICS RESEARCH Section A
www.elsevier.com/locate/nima

Gamma-ray imaging with a coaxial HPGe detector

T. Niedermayr[a], K. Vetter[a,*], L. Mihailescu[a], G.J. Schmid[a], D. Beckedahl[a], J. Blair[b], J. Kammeraad[a]

[a]*Lawrence Livermore National Laboratory, Livermore, CA 94550, USA*
[b]*Bechtel Nevada, North Las Vegas, NV 892310, USA*

Received 18 June 2005; received in revised form 12 July 2005; accepted 12 July 2005
Available online 15 August 2005

Abstract

We report on the first experimental demonstration of Compton imaging of gamma-rays with a single coaxial high-purity germanium (HPGe) detector. This imaging capability is realized by two-dimensional segmentation of the outside contact in combination with digital pulse-shape analysis, which enables to image gamma-rays in 4π without employing a collimator. We are able to demonstrate the ability to image the 662 keV gamma-ray from a ^{137}Cs source with preliminary event selection, with an angular resolution of 5° and a relative efficiency of 0.3%. This efficiency expresses the fraction of gamma-rays that can be imaged, out of the total gamma-ray flux which is emitted into the solid angle of the detector. In addition to the 4π imaging capability, such a system is characterized by its excellent energy resolution and can be implemented in any size possible for Ge detectors to achieve high efficiency.

PACS: 29.30.Kv; 29.40.Wk; 29.40.Gx; 89.20.+a

Keywords: Gamma-ray imaging; Segmented HPGe detector; Compton camera

1. Introduction

The ability to image and characterize known as well as unknown gamma-ray sources is finding a variety of applications in biomedical research and nuclear medicine, astrophysics, national security, such as nuclear nonproliferation, stockpile stewardship, nuclear waste monitoring and, most recently, nuclear counterterrorism. While gamma-ray imaging is an established tool in nuclear medicine or astrophysics, only recently has the impact of gamma-ray imaging for nuclear security applications been recognized. Here, the goal is to provide improved capabilities to detect, localize, and characterize nuclear materials. One of the outstanding challenges in homeland security is the

*Corresponding author at: Glenn T. Seaborg Institute, Lawrence Livermore National Laboratory, L-231, 7000 East Avenue, Livermore, CA 94550, USA. Tel.: +1 925 423 8663; fax: +1 925 422 3160.
E-mail address: kvetter@llnl.gov (K. Vetter).

0168-9002/$ - see front matter © 2005 Elsevier B.V. All rights reserved.
doi:10.1016/j.nima.2005.07.017

detection and identification of nuclear threats in the midst of a sea of non-threat objects, which consists of legitimate radioactive objects commonly found in commerce and environment. In addition to the detection of nuclear materials which can be achieved by simple counting instruments, it is crucial to obtain as much information from this material as possible to mitigate the primarily nuisance alarms. This can be achieved by identifying the radioisotope via its characteristic gamma-ray decay, and by imaging it, e.g. by measuring the location and the shape of sources. In addition to the ability to localize and image gamma-ray sources, gamma-ray imaging can potentially increase the sensitivity in finding such sources, particularly in complex and changing backgrounds, due to the ability to improve signal-to-background. In particular, collimator-less Compton imaging systems enable to measure signals and background simultaneously, and therefore potentially provide the biggest gain in signal-to-background. Gamma-ray imagers based on position-sensitive semiconductor detectors such as high-purity Ge (HPGe) provide excellent imaging and spectroscopic characteristics and therefore fulfill both important requirements in national security.

Well-established means of imaging consist of a mechanical and passive collimator such as parallel-hole or pinhole systems in front of a position-sensitive gamma-ray detectors [1]. These systems suffer from the trade-off between efficiency and resolution. More advanced collimator- or aperture-based instruments consist of modulated apertures either in space-coded aperture or time-rotation modulation aperture, which have limited capabilities in high-activity and complex backgrounds. The ideal gamma-ray imager, a gamma-ray lens, is very difficult to realize due to the small angle of total reflection. Multilayer, diffractive optics system that have been built are able to focus gamma-rays up to 160 keV; however, these systems are characterized by a large focal length and a small field of view [2]. An alternate way to image gamma-rays without the use of a collimator is Compton imaging. Recent advances in the two-dimensional segmentation of semiconductor detectors along with signal processing allow us now to build efficient and high-resolution Compton imaging systems.

We report on one possible implementation, which consists of a two-dimensionally segmented, coaxial HPGe detector. Other approaches consist of planar configurations made of a variety of materials such as Si, Ge, or CdZnTe, either in double-sided strip or pixelated geometry [3–5]. The advantage of a coaxial HPGe detector is the large volume of a single detector that can be manufactured, which translates into high efficiencies for gamma-ray energies up to several MeV. In addition, intrinsic properties of high-purity Ge enable excellent energy resolution and signal–noise ratios. The atomic number of $Z = 32$ represents an acceptable compromise between efficiency, which requires high-Z, and Compton imaging sensitivity which requires low Z. The latter is due to the fact that for Compton imaging at least one Compton scatter process is required before the gamma-ray is absorbed via the photoelectric effect, and the two first interactions have to be sufficiently far apart that one is able to separate them and is able to deduce the scattering angle with finite accuracy.

In the following, we will briefly introduce the concept of Compton imaging in Ge detectors. In Section 3, we will introduce the 40-fold segmented coaxial HPGe detector, which was built by ORTEC and used for our experiments. In Section 4 we discuss pulse-shape analysis procedures to deduce three-dimensional positions for individual gamma-ray interactions. Section 5 finally illustrates measurements, which demonstrate Compton imaging in such a detector and discusses the impact of improvements in the pulse-shape analysis of multiple interactions, which occur close to each other.

2. Compton imaging with a HPGe detector

As first published by Todd for nuclear medicine [6] and Schönfelder for astrophysics [7], the concept of Compton imaging relies on the Compton scattering process, and the relationship between the scattering angle θ, the energy of the incident gamma-ray E_γ, and the energy of the first

interaction E_1 which is

$$\cos(\theta) = 1 + \frac{511}{E_\gamma} - \frac{511}{E'_\gamma} \leftrightarrows, \quad E'_\gamma = E_\gamma - E_1.$$

As illustrated in Fig. 1, the scattering angle describes a cone whose symmetry axis is defined by the line connecting positions of the first two interactions. The projection of those cones on a sphere will overlap at the source location when many events are imaged or back-projected. Without measuring the direction of the Compton electron, the incident angle of the gamma-ray can only be determined to be on a cone surface. Since in Ge the range of electrons is typically below 1 mm (e.g., a 1 MeV gamma-ray generates an electron of about 500 keV which has a range of about 0.5 mm in Ge), it is very difficult to measure the scattering angle of the electron, particularly considering the complex slowing-down process of electrons. Only in low-Z or low-density detectors, such as gases at a pressure of about 1 atm, electron vertices could be measured [8]. However, the efficiency to induce a gamma-ray interaction at all in these instruments is extremely low.

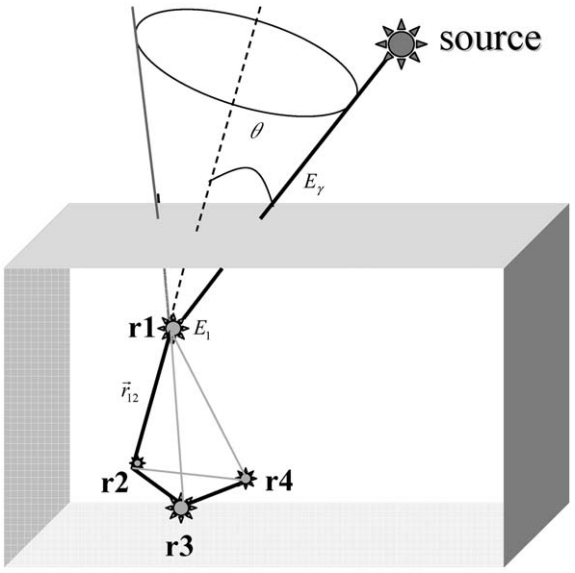

Fig. 1. Illustration of the Compton imaging principle. Positions of the first two interactions define the symmetry axis of a cone whose opening angle is defined by the energy of the first interaction and the total gamma-ray energy.

The angular resolution that can be obtained in Compton imaging depends on uncertainties in the determination of positions of interactions and deposited energies. The error in positions affects the cone axis direction while the error in energies affects the angle θ of the cone. The position and energy resolution can, in principle, be improved for better angular resolution but the electron on which the photon Compton scatters carries momentum, which is inherently unknown and will limit the best angular resolution attainable [9]. In order to improve image quality, a large number of image reconstruction algorithms have been developed [10–13]. The iterative list-mode maximum-likelihood (LMML) algorithm, which is well-suited for low statistics data can improve angular resolution, as shown later.

In Ge, Compton scattering is the dominant interaction process between 150 keV and about 8 MeV. However, at low energies, e.g. below 300 keV, the energy of the scattered gamma-ray is so low that in most of the cases it is absorbed by the photoelectric effect within 2 mm, which makes it very difficult to identify two interactions and separate them. But, even if they can be separated, the uncertainty in the position measurement, particularly if based on pulse-shape analysis at low energies, will limit the angular resolution significantly. This is one reason which explains why previous attempts to use coaxial Ge detectors as Compton imagers failed [14]. For gamma-ray energies of 500 keV a higher angular resolution of a few degrees should be readily achievable. For gamma-ray energies above 1 MeV the angular resolution should be even better and ultimately limited only by the range of the Compton scattered electron.

If only two interactions are involved in the event, a simple energy-ratio consideration can identify which of the two interactions is most likely the first one [15]. For higher gamma-ray energies, i.e. 500 keV, two and more Compton scattering processes become more likely before the gamma-ray is absorbed. To obtain the proper scattering sequence, gamma-ray tracking algorithms have to be employed [16–18]. These gamma-ray tracking algorithms not only provide the most likely scattering sequence, but also

provide the likelihood of a full-energy deposition or an escape event, which means that the gamma-ray was not fully absorbed in the detector but escaped before. In this way, they can improve the spectroscopic response of the detector, e.g. by increasing the peak-to-total ratio [16].

In summary, the full volume imager combines high efficiency and high energy resolution but is limited by the separation ability of events which scatter close by, and reduces the ultimately achievable angular resolution to a few degrees.

3. Coaxial HPGe prototype imager

In the approach presented here, three-dimensional positions and energies of gamma-ray interactions are obtained by pulse-shape analysis in a two-dimensionally segmented, coaxial HPGe detector, which was manufactured by ORTEC. The closed-end crystal is of n-type with the segmented B-contact outside and the unsegmented Li-contact inside. The impurity concentration was provided by the manufacturer to be $5 \times 10^{-9}\,\mathrm{cm}^{-3}$ in the front and $10 \times 10^{-9}\,\mathrm{cm}^{-3}$ in the back of the crystal. The crystal's diameter is 5 cm, the overall length 8 cm. It is segmented 40-fold on the outside cylindrical surface only to simplify pulse-shape analysis: eight longitudinal segments separated by $\Delta\varphi = 45^{\circ}$ (labeled A through H) and five transverse segments separated by $\Delta z = 1\,\mathrm{cm}$ (labeled 1 through 5), as illustrated in Fig. 2. The B-contact at the front 2 cm which contains the complex, pseudo-planar electrical fields, and the rear 1 cm were left without segmentation. The crystal is oriented in such a way as to have the major crystallographic axes aligned with the segmentation lines. This results in a similar charge collection with respect to the azimuthal angle and avoids transfer of charge carriers from one electrode to another during the collection process. This simplifies the simulation of charge transport and signal shapes. Custom preamplifiers built around warm FETs are mounted on a circular motherboard close to the detector to reduce input capacitance. A picture of the detector aluminum housing with the preamplifiers visible is also shown in Fig. 2. A digital signal acquisition system manufactured by Struck Innovative Systems (SIS) is used to read out the 40 segment channels, as well as the front and the central contact, with a 100 MHz sampling rate and 12 bit ADCs. Data from the eight-channel digitizer boards are read through a VME-PCI interface, and processed and analyzed on a PC. The typical energy resolution obtained is 0.9 and 1.9 keV at gamma-ray energies of 60 and 1332 keV, respectively, at a peaking time of 4 μs. The energy resolution of the central channel was degraded to about 2.5 keV at 60 keV, due to the leakage current on the rear

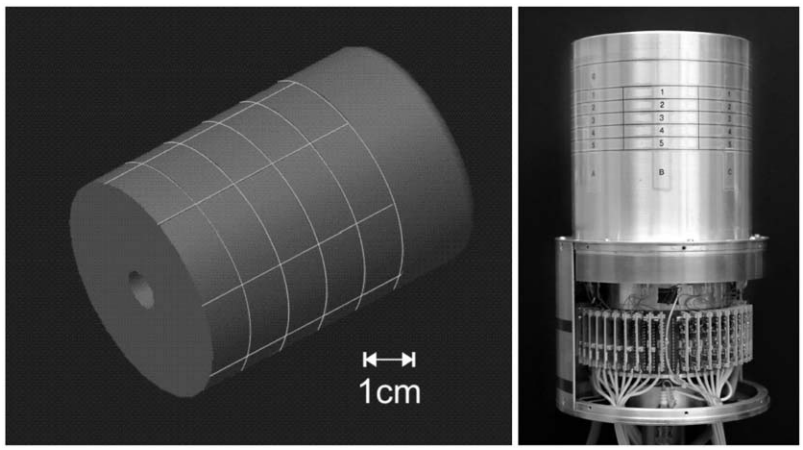

Fig. 2. Coaxial HPGe detector, 40-fold segmented. The segmentation scheme is indicated on the left; the detector housing and the preamplifier arrangement can be seen on the right.

side of the Ge detector. The degradation could have been prevented by isolating the rear and non-segmented side by electrically segmenting the inner contact.

4. Position determination through pulse-shape analysis

In order to determine 3-D positions of interaction sites of a gamma-ray inside a detector, a detailed understanding of the resulting pulse-shapes is necessary. The shape of the signal generated on the charge collecting electrode, as well as the shape of the induced signals produced on the neighboring electrodes, is a unique signature of the 3-D position of the interaction.

When gamma-ray photons interact in Ge, they can produce a recoil electron or a photoelectron at each interaction site. These electrons will lose about a third of their energy by generating electron–hole pairs and two-thirds by exciting lattice vibrations. The charge cloud which is left along the track of the primary electron has a size on the order of the stopping distance. In the following, the charge cloud is considered to be generated instantaneously and its extent is neglected in simulations. The lateral diffusion of charge carriers perpendicular to the electrical field is neglected as well, since the maximum range can be estimated to be smaller than 100 μm, which is small compared to the overall dimensions of segments considered in the detector.

A signal is produced by the charge cloud by inducing an image charge of opposite polarity at the electrodes. The charge is accelerated under the influence of the applied electric field and reaches an equilibrium velocity, which is considered here to be reached instantaneously for simplification. This charge drift in the detector induces a change in the image charge at the electrodes. If the charge is produced far away from the destination electrode, the induced charge is distributed over several electrodes. As the charge moves closer to its destination electrode, the charge is increased on the collecting electrode, and the induced charge on the neighboring electrodes decreases until the charge finally reaches the destination electrodes. Thus a net charge is only measured on the destination electrode, while the neighboring electrodes have transient signals which vanish when the charges are collected.

The first step in calculating signals that can be observed at the segments is the determination of the path of charge carriers inside the detector volume for a given position of interaction. The charge migrates under the influence of the applied electric field, which depends on the detector geometry, applied voltage, intrinsic space-charge density ρ and carrier mobility μ. The electric field is calculated for the detector geometry by solving the Poisson equation using the finite-element method program MAXWELL-3D:

$$\Delta\phi(\vec{r}) = \frac{-\rho(z)}{\varepsilon}.$$

An electric potential is thus obtained for the three-dimensional detector volume with a Cartesian grid size of 1 mm. The electric field can then be calculated by

$$\vec{E}(\vec{r}) = -\nabla\phi(\vec{r}).$$

The trajectory of the electrons and holes can be calculated using the velocity

$$\vec{v}(\vec{r}) = \mu\vec{E}(\vec{r}).$$

The electric field is interpolated between grid points. A time interval of 10 ns is used in generating the charge carrier trajectories, small enough to prevent any drift velocities discontinuities. The charge carrier mobility depends on the temperature, electric field, the angle between the drift velocity and crystal orientation and, additionally, on the angle between the electric field and crystal orientation [19,20]. The latter dependency is not taken into account here due to the difficulty in a closed description for the hole mobility, which implies that charge carriers are only allowed to move along the electrical field.

The next step in calculating the signals generated at electrodes is to calculate the weighting potential [21,22]. The Laplace equation is solved with voltage applied only on the collecting electrode and all the other contacts grounded. By calculating the electric field for each grid point and electrode, and using the previously calculated

charge carrier trajectories, the induced charge can be obtained with

$$\Delta Q_{i,j} = \frac{q_0 \vec{E}_j(\vec{r}_i)\Delta\vec{r}_i}{V_0},$$

where q_0 is the charge deposited and V_0 the applied voltage. Thus, for each 1835 positions on the 1 mm grid in each segment, the signals generated at each electrode have been calculated. These signals are used to determine the positions of interactions, e.g. by least-square minimization procedures.

5. Experimental imaging with the coaxial detector

5.1. Signal mapping measurements

In order to validate and adjust the simulated signals, measurements resulting from interactions with defined positions were carried out. In order to restrict interactions to Compton scatters at 90° along a line in the HPGe coaxial imager, a collimated source was used and a HPGe coaxial "catcher" detector was operated in coincidence. The experimental setup is shown in Fig. 3. A ^{137}Cs point source is collimated behind two hevimet bricks separated by 1.5 mm, thus forming a plane parallel to the detector transverse direction z. A coaxial HPGe "catcher" detector is placed behind two hevimet bricks separated by 1.5 mm, defining a plane of sight at 90° in respect to the source illumination plane. A line of possible interactions is thus defined by the intersection of these two planes, parallel to the imager z axis, with a diameter of approximately 2 mm. In order to restrict events to ^{137}Cs 662 keV photons scattering at 90° in the imager and subsequently absorbed in the "catcher" detector, the "catcher" detector was operated in coincidence with the imager and energy gates were set on both detectors. Thus, only events, which deposit 374 keV in the imager and 278 keV in the "catcher" were recorded. The "catcher" detector was shielded with lead in order to reduce false or random coincidences. Monte Carlo simulations show that more than 90% of all coincidence events measured in this way are due to single interaction events in the imager. Both hevimet collimators are mounted on translation stages in order to scan the imager in two dimensions, which was done on 12 different positions on a 3 mm grid, as shown in Fig. 4. Due to symmetry considerations, these 12 positions are sufficient to characterize the whole detector volume. The overall alignment was determined by matching intensity ratios of differ-

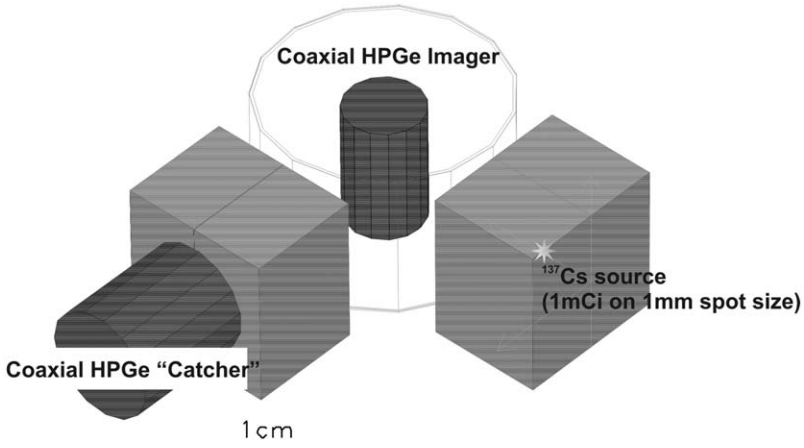

Fig. 3. Coincidence setup used to map out signals within the detector. A 1 mCi ^{137}Cs source is located in a hevimet block with a slit opening of 1.5 mm to define a plane of interactions in the detector. At 90°, a second HPGe detector is mounted behind another hevimet absorber with a slit opening of 1.5 mm. These slits define a line of possible interactions when a coincidence between the coaxial imager and the coaxial catcher detector is required.

ent segments which proved to be accurate to better than 1 mm.

Out of the five illuminated segments F1,…,F5 (where F corresponds to the longitudinal position and 5 to the transverse position), only events in the middle three (F2,…,F4) were saved in order to be able to record the signal on the charge collecting electrode, as well as the induced signals on all of the eight neighboring electrodes. The measured energy correlation between the imager and "catcher" detectors is shown in Fig. 5. The shape and width of the peak is determined by the Compton profile in Ge reflecting the electron momentum on which the photon Compton scatters.

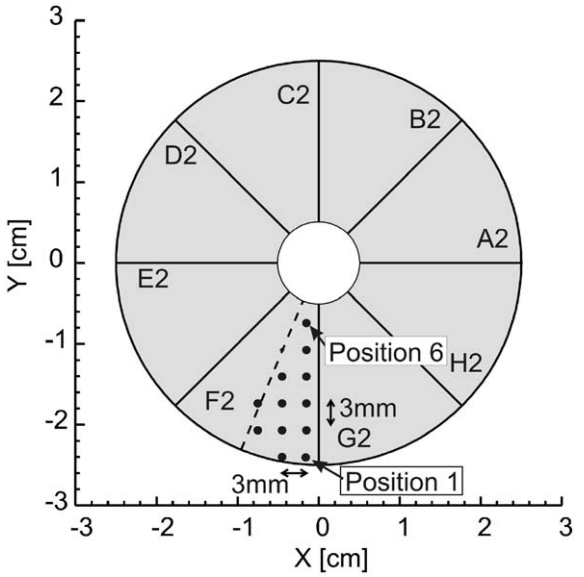

Fig. 4. 12 X–Y positions of the collimator during coincidence measurements. Segments F1–F5 were illuminated, while only segments F2–F4 were used in the trigger.

Since the experimental setup only provides a line of interactions in the detector, the point of interaction has to be inferred by the amplitude of signals. This is done by calibrating the signal position in accordance with the range of amplitudes. The advantage of this experimental procedure, compared to reducing the interaction sites to a point, is a large reduction in the number of necessary measurements and therefore measurement time. In Fig. 6, signals from the charge collecting electrode and its eight neighbors is shown for two different positions. The induced signals are crucial in order to determine the 3D position of the interaction. They can have either polarity, depending on the radius of the interaction, which determines if electrons or holes will dominate in the signal. On one hand, this has the advantage of increasing the dynamic range of signals, thereby potentially increasing the position sensitivity. On the other hand, the induced signals from electrons and holes can cancel each other out for interactions in certain areas of the segment,

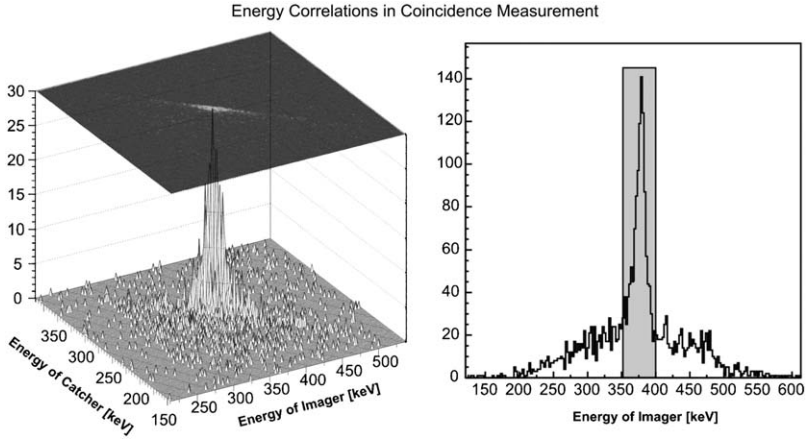

Fig. 5. Measured energy correlation between imager and catcher detector.

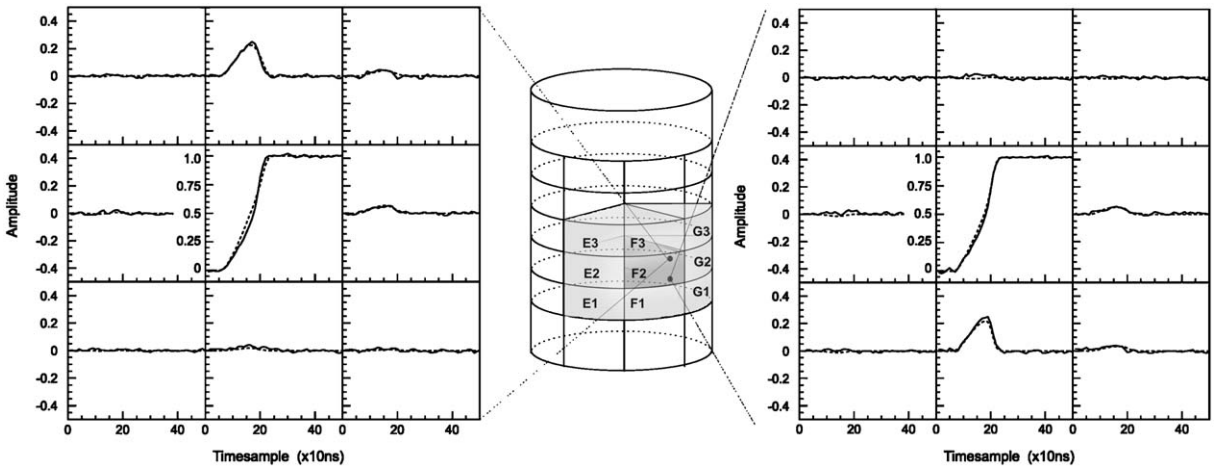

Fig. 6. Set of segment signals for two locations indicated in the middle. Signals on the left reflect an interaction closer to the upper segment F3, the interaction on the right is closer to the lower segment F1. The solid lines are measured, the dashed lines calculated signals.

thus decreasing the sensitivity there. Since the position of the interaction in measurements is not restricted to a point but to a line parallel to the longitudinal segmentation, a set of signals with different amplitudes on top and bottom and similar amplitudes left and right are recorded.

In order to validate the simulated signals, calibration signals are treated as unknown data for which the positions must be determined. In this way the position resolution of the system can be determined, since the position of the measured signals is known. The measured signals are fitted with simulated signals using a χ^2 minimization procedure. The reconstructed, three-dimensional positions for six out of the 12 collimator positions are shown in Fig. 7. As discussed before, an energy deposition of 374 keV was required in segments F2, F3 or F4 and the fit was performed on an event-by-event basis using signals of nine segments. Although the fitting algorithm provides excellent agreement between measured and calculated signals, inhomogeneous distributions of positions and deviations of up to 3 mm can be observed. The reconstructed positions are shifted towards segment boundaries, e.g. areas of higher sensitivity. These effects are due to the reduced sensitivity in the middle of the segments (regions furthest away from the electrode edges).

5.2. Compton imaging

To demonstrate the imaging capabilities, measurements were carried out by illuminating the detector with a ^{137}Cs source two meters away. Only events which deposit the full gamma-ray energy in the three middle layers were considered, to ensure that all segments hit have a complete set of neighbor signals. In addition, the interactions were required to take place in two different segments separated by a distance large enough in order to be able to fit the measured signals and thus extract the energy and location of events. In practice, this meant a separation of at least two segments between active segments. In our experiment, 0.4% of all events collected fulfilled these conditions. This is in fair agreement with 0.8% expected by Monte-Carlo simulations performed with GEANT [23]. Fig. 8 shows energy and position distributions of the high- and low-energy events. The first interaction, closer to the source, is the one with low energy, as expected for 662 keV photons. With positions and energies determined, it is possible to reconstruct an image with simple cone back-projection. The resulting image is shown on the left hand side in Fig. 9. By applying a list-mode maximum-likelihood algorithm [24], the image on the right of Fig. 9 is obtained after

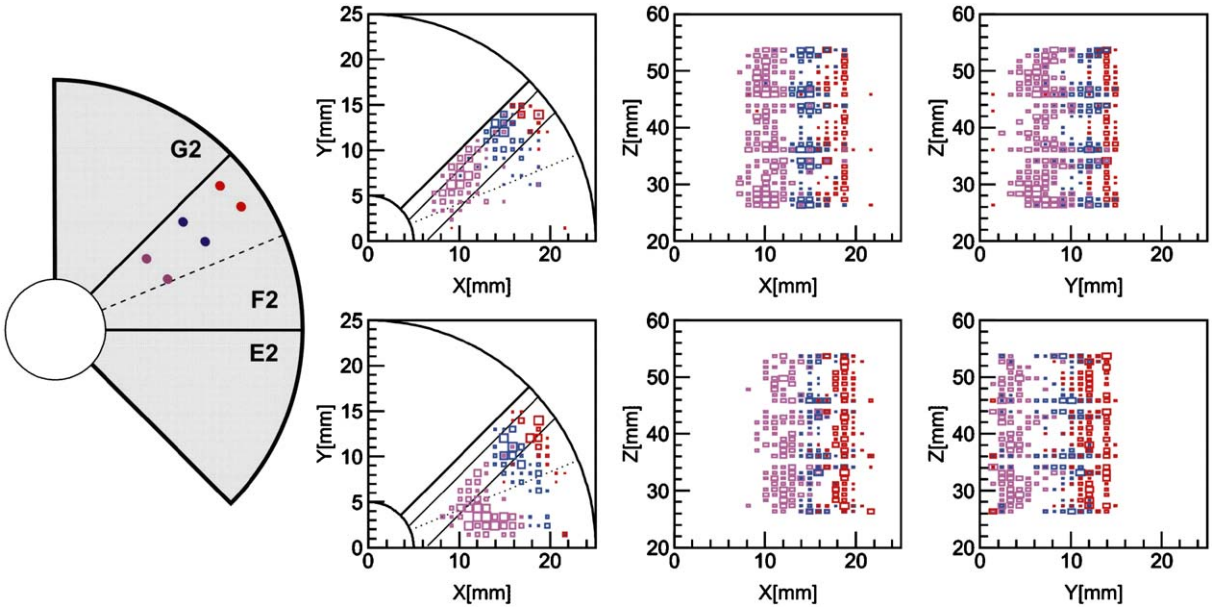

Fig. 7. Location of collimator positions (left) and corresponding deduced positions by signal decomposition calculations (right). The top row on the right reflects positions on the line closer to segment G2.

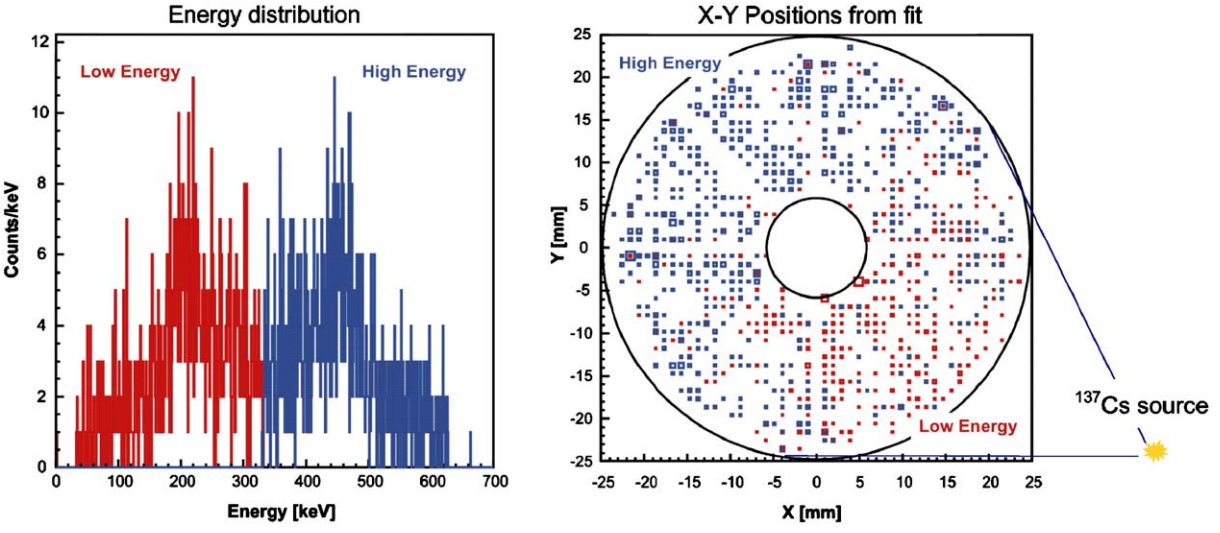

Fig. 8. Energies (left) and positions (right) identified and determined by signal decomposition calculations after illuminating the detector with a ^{137}Cs source as indicated on the right. The light boxes indicate low energies and therefore the first of two interactions.

ten iterations, resulting in an angular resolution of about 5°.

Monte-Carlo simulations mentioned above indicate that about 80% of all gamma-rays emitted in the solid angle of the detector interact with the detector, which means that the overall imaging efficiency for the implemented event selection, which resulted in an angular resolution of 5°, is about 0.3%. This efficiency expresses the fraction of gamma-rays, which can be imaged out of the

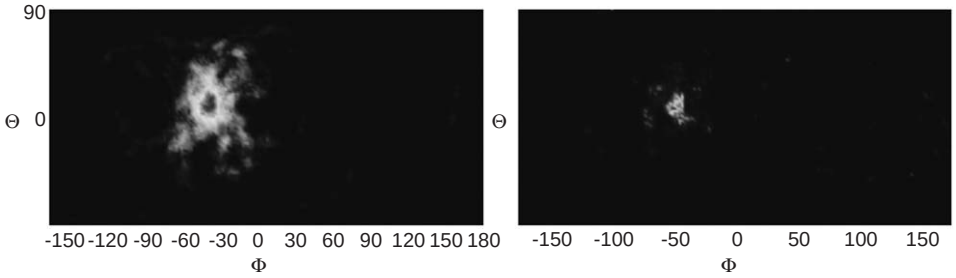

Fig. 9. Images deduced by measured energies and positions of two interactions in the detector. The left image was determined with simple cone back-projection, the image on the right was obtained with an iterative list-mode maximum-likelihood method.

total gamma-ray flux, that is emitted into the solid angle of the detector. More sophisticated signal-decomposition methods, which enable the analysis of multiple interactions in one or adjacent segments, should be able to increase the sensitivity to levels larger than 1%. Assuming the position resolution of 3 mm as achieved so far, the angular resolution will degrade to about 10°. However, if the position resolution can be improved to 1 mm, the previous angular resolution of 5° can be achieved with an efficiency of 5%

6. Conclusion

We have demonstrated Compton imaging in a two-dimensionally segmented, coaxial HPGe detector by using pulse-shape analysis to deduce three-dimensional positions of interactions. With simple event-selection criteria, we obtain about 5° angular resolution at an energy of 662 keV with a relative efficiency of 3×10^{-3}. Monte-Carlo simulations indicate that with more sophisticated signal-decomposition methods, which enable the analysis of multiple interactions in one or adjacent segments, it should be possible to increase the sensitivity to levels larger than 1%. Assuming the position resolution of 3 mm as achieved so far, the angular resolution will degrade to about 10°. However, if the position resolution can be improved to 1 mm, the angular resolution of 5° can be achieved with an efficiency of 5%.

With the excellent intrinsic properties for gamma-ray spectroscopy of a coaxial HPGe detector and, now in addition, the 4π-imaging capability with a sensitivity of larger than 1% and a resolution of about 5°, such an instrument becomes attractive for a variety of applications, e.g. for nuclear materials monitoring or emergency response.

Acknowledgements

We thank Pat Sangsingkeow from ORTEC for her support in the endeavor of making this detector work. Special thanks to Harold Yaver and Michael Maier from Lawrence Berkeley National Laboratory for the hard work on the preamplifiers.

The work was performed under the auspices of the US Department of Energy by University of California Lawrence Livermore National Laboratory under Contract no. W-7405-Eng-48.

References

[1] J.A. Sorenson, M. Phelps, Physics in Nuclear Medicine, second ed., W. B. Saunders Company, Philadelphia, PA, 1987.
[2] D.L. Windt, et al., Appl. Opt. 42 (2003) 2415.
[3] Y. Du, Z. He, G.F. Knoll, D.K. Wehe, W. Li, Nucl. Instr. and Meth. A 457 (2001) 203.
[4] B.F. Phlips, et al., IEEE Trans. Nucl. Sci. NS-43 (1996) 1472.
[5] K. Vetter, M. Burks, L. Mihailescu, Nucl. Instr. Meth. Phys. Res. A 525 (2004) 322.
[6] R.W. Todd, J.M. Nightingale, D.B. Everett, Nature 251 (1974) 132.
[7] V. Schoenfelder, et al., Nucl. Instr. and Meth. 107 (1973) 385.
[8] R. Bellazzini, et al., Nucl. Instr. and Meth. 535 (2004) 477.

[9] D. Brusa, et al., Nucl. Instr. and Meth. 379 (1996) 167.
[10] L. Parra, H.H. Barrett, IEEE Trans. Nucl. Sci. NS-17 (1998) 228.
[11] L.A. Shepp, Y. Vardi, IEEE Trans. Nucl. Sci. NS-1 (1982) 113.
[12] S.J. Wilderman, et al., IEEE Trans. Nucl. Sci. NS-48 (2001) 111.
[13] R. Basko, G.L. Zeng, G.T. Gullberg, Phys. Med. Biol. 43 (1998) 887.
[14] G.J. Schmid, D.A. Beckedahl, J.J. Blair, J.E. Kammeraad, K. Vetter, A. Kuhn, Nucl. Instr. and Meth. A 459 (2001) 565.
[15] C.E. Lehner, Z. He, F. Zhang, IEEE Trans. Nucl. Sci. NS-51 (2004) 1618.
[16] G.J. Schmid, et al., Nucl. Instr. and Meth. A 430 (1999) 69.
[17] G.J. Schmid, et al., IEEE Trans. Nucl. Sci. NS-44 (1997) 975.
[18] J. van der Marel, B. Cederwall, Nucl. Instr. and Meth. A 437 (1999) 538.
[19] G. Ottaviani, C. Canali, A. Albergi Quaranta, IEEE Trans. Nucl. Sci. NS-22 (1975) 192.
[20] L. Reggiani, C. Canali, F. Nava, G. Ottaviani, Phys. Rev. B 16 (1977) 2781.
[21] S. Ramo, Proc. IRE 27 (1939) 584.
[22] G.F. Knoll, Radiation Detection and Measurement, third ed., Wiley, New York, 2000.
[23] GEANT3, Detector Description and Simulation Tool, CERN, Geneva, 1993.
[24] L. Mihailescu, et al., Nucl. Instr. and Meth. submitted for publication.